doi:10.1016/j.jmb.2011.04.012 J. Mol. Biol. (2011) 410, 667–680

Contents lists available at www.sciencedirect.com

Journal of Molecular Biology

journal homepage: http://ees.elsevier.com.jmb

Structure and Stoichiometry of Template-Directed Recombinant HIV-1 Gag Particles

Nancy L. Goicochea[1], Siddhartha A. K. Datta[2], Murali Ayaluru[3], Cheng Kao[3], Alan Rein[2]* and Bogdan Dragnea[1]*

[1]*Department of Chemistry, Indiana University, Bloomington, IN 47405, USA*
[2]*HIV Drug Resistance Program, National Cancer Institute, Frederick, MD 21702-1201, USA*
[3]*Department of Biology, Indiana University, Bloomington, IN 47405, USA*

Received 20 November 2010; received in revised form 5 April 2011; accepted 6 April 2011

Edited by M. F. Summers

Keywords:
HIV Gag;
nanoparticle;
templated virus assembly;
liquid crystal;
electron microscopy

Size polydispersity of immature human immunodeficiency virus type 1 (HIV-1) particles represents a challenge for traditional methods of biological ultrastructural analysis. An *in vitro* model for immature HIV-1 particles constructed from recombinant Gag proteins lacking residues 16–99 and the p6 domain assembled around spherical nanoparticles functionalized with DNA. This template-directed assembly approach led to a significant reduction in size polydispersity and revealed previously unknown structural features of immature-like HIV-1 particles. Electron microscopy and image reconstruction of these particles suggest that the Gag shell formed from different protein regions that are connected by a "scar"—an extended defect connecting the edges of two continuous, regularly packed protein layers. Thus, instead of a holey protein array, the experimental model presented here appears to consist of a continuous array of ~5000 proteins enveloping the core, in which regular regions are separated by extended areas of disorder.

Introduction

Virus assembly, maturation, and disassembly are processes that constitute possible targets for antiviral therapy. A detailed knowledge of the structural properties of viruses and their assembly intermediates is necessary to understand and interfere with these stages of the virus life cycle. A case in point is the human immunodeficiency virus type 1 (HIV-1),[1–4] which, despite intense study for more than 25 years, still presents challenges coming from a limited knowledge of its architecture and the transformations associated with its passage from the noninfectious immature state to the infectious mature state during the viral life cycle.

The major structural element of HIV-1, the Gag polyprotein, contains four major domains: the matrix (MA), capsid (CA), nucleocapsid (NC), and the C-terminal p6.[5] The p6 domain is not required for virus particle assembly. The HIV-1 Gag assembles into an immature particle in which the monomers are rod shaped and arranged radially, with the N-terminus of the MA domain oriented toward the membrane bilayer through a myristate modification and with the C-terminal NC domain pointing toward the particle center, presumably in contact with RNA.[6,7] Upon assembly and budding, the viral protease PR cleaves the Gag molecules to induce a dramatic rearrangement of the Gag-derived

*Corresponding authors. E-mail addresses: reina@mail.nih.gov; dragnea@indiana.edu.

Abbreviations used: HIV-1, human immunodeficiency virus type 1; MA, matrix; CA, capsid; NC, nucleocapsid; VLP, virus-like particle; TEM, transmission electron microscopy; PEG, polyethylene glycol; ss, single-stranded; DLS, dynamic light scattering; EM, electron microscopy; 3D, three-dimensional; MWCO, molecular weight cutoff.

products, in which CA reassembles into a conical-shaped capsid structure. Inhibition of the HIV maturation process, primarily targeting the PR protein, has emerged as one element in highly effective antiretroviral therapy. Additional steps in HIV capsid assembly also show promise, as therapeutic targets and new drugs have been structure-based designed to interfere with the Gag cleavage points.[8–10] As a consequence, determining the ultrastructural features of immature and mature viral particles will accelerate the discovery process of such therapies.

While atomic-level resolution structures of isolated, individual Gag domains have been described in detail,[11–17] the quaternary structures of the capsid and, in particular, of the Gag domain contacts in the immature virus remain unclear.[18,19]

In vitro assembly of HIV-1 Gag with nucleic acid results in virus-like particles (VLPs) that share similar structural properties with immature HIV-1 virus particles isolated from cells.[5,18–22] Thus, Gag VLPs have been proposed as a simple and reliable model for the study of Gag–Gag interactions in immature HIV particles. Recent cryoelectron tomography studies of Gag VLPs and authentic immature virus particles provided the current working model for the Gag arrangement within the protein lattice.[18] The model is briefly introduced in the following.

The minimal set of required components for *in vitro* assembly of Gag VLPs is the HIV Gag polyprotein or assembly competent recombinant versions of Gag, such as Δ16–99 Gag[20,22] and a source of nucleic acid. The deleted Δ16–99 Gag assembles *in vitro* with greater efficiency than its undeleted counterpart. The reason for this improved efficiency in assembly is not well understood, but studies suggest that the presence of the MA domain inhibits efficient assembly *in vivo* and *in vitro*.[23] The VLPs assembled *in vitro* from the deleted Gag protein have been characterized in detail,[18,22] and their lattice structure appears essentially identical to that in immature particles assembled in mammalian cells. In essence, this is a hexameric lattice of Gag monomers in contact with each other via their CA domains. Curvature is apparently introduced into the lattice not by insertion of pentameric "defects", as in icosahedral viruses, but by gaps.[18,19,24]

Although by transmission electron microscopy (TEM) Gag VLPs assembled *in vitro* are more regular in appearance than immature HIV, their size distribution can still be broad or multimodal.[7] Size polydispersity represents a challenge for ultrastructural analysis since, with the exception of cryoelectron tomography, all structural methods involve at some level averaging among a statistical ensemble of particles.

The hypothesis for the work presented here was that template-directed assembly of Gag around a spherical nanoparticle core should reduce the size polydispersity and thus improve access to previously unknown structural features of the immature particle. An excellent example of natural virus templating is found in the bluetongue virus structure,[25] where the VP37 outer shell is assumed to assemble on a smooth 120 subunit inner protein shell.[26] In our case, Gag quasi-spherical shells (Au-Gag VLPs) were prepared by self-assembly of recombinant Gag protein with spherical gold nanoparticles functionalized with single-stranded (ss)-DNA. Ligand-coated gold nanoparticles have been previously reported as suitable templates for directed *in vitro* assembly of icosahedral VLPs.[27–29] In the Gag case, the presence of immobilized DNA on the spherical template was required for assembly. The Gag shell of Au-Gag VLPs displayed a much more uniform appearance than authentic immature VLPs or VLPs assembled on free nucleic acid *in vitro*; this enabled the use of models for higher structural analysis. While previous reports determined that immature particles and Gag VLPs contained incomplete Gag shells covering roughly ~40–60% of the surface of the particles,[18,19,24] the shell of the Au-Gag VLPs was largely complete. However, the homogeneous distribution of Gag around the nanoparticle core was interrupted by an extended defect defined as a region of lower density or "scar", spanning approximately half of the particle circumference. This defect seems to originate from shell edge overlapping and affects roughly 30% of the entire area of the sphere. We consider possible explanations for this observation.

Results

Nanoparticle functionalization and *in vitro* assembly with recombinant HIV-1 Gag

In order to form templates for *in vitro* assembly of VLPs, gold particles (40 nm, 50 nm, 60 nm, and 80 nm diameter) were functionalized with thiol-modified polyethylene glycol (PEG)-derived ss-DNA (Fig. S1). Different sizes of spherical gold were chosen to test the possibility that an optimal template curvature would improve monodispersity and morphology of Gag virus particles. The thiol group present at one terminus of the PEG provides binding specificity for the nanoparticle surface. The other terminus of the PEG chain was connected to the 5′ end of the 50-base oligodeoxynucleotide $d(TG)_{25}$. [HIV-1 NC protein binds with particularly high affinity to the repeating sequence $d(TG)_n$[30,31]]. Thus, the DNA was tethered to the particle with a flexible, hydrophilic stalk, ~ 1.6 nm long. DNA-PEG-Au conjugates prepared with different sizes of gold were mixed with recombinant HIV-1 Gag

and were dialyzed against low ionic strength buffer to produce Au-Gag VLPs (Fig. S2, step 1).

The hydrodynamic particle diameter was measured after DNA conjugation using dynamic light scattering (DLS). DLS measurements of the hydrodynamic radius of Au-Gag VLPs as a function of the DNA-PEG-Au conjugate diameter are presented in Fig. 1a. The trend followed by the experimental points is remarkably linear, and the 45° angle formed between the slope of the least-square fit line and the *x*-axis suggests that VLP sizes increase linearly with gold diameter. Two consequences of this proportionality are as follows: (a) protein–core association does not seem to be biased by triangulation number constraints as is typically the case for icosahedral plant viruses[27,29,32,33] and (b) the thickness of the Gag layer when forming VLPs could be approximated from the intercept value (intercept = 2 Gag lengths) of the linear equation and was estimated at 15.4 nm. Figure 1a also shows the expected diameters for *T*-numbers between 1 and 48; while we cannot exclude the possibility that Au-Gag VLP diameters are discretized by the constraint of specific *T*-numbers, there is no suggestion of such a trend in the data.

The association of gold nanoparticles with HIV-1 Gag was further analyzed by native agarose gel electrophoresis (Fig. 1b). Before assembly, the basic Gag protein (lane 3) migrated with a net positive charge. The basic NC domain of Gag interacts electrostatically with the phosphate backbone of the nucleic acid coat on the templating DNA-PEG-Au nanoparticles during Au-Gag VLP assembly; after assembly, the Au-Gag VLPs (lane 1) had slight a negative charge. As expected, the mobility of Au-Gag VLPs was lower than that of DNA-PEG-Au conjugates (lane 2) due to their larger size and smaller net charge. While assembly took place regardless of the size of the nanoparticle, VLPs did not form when the gold nanoparticles were functionalized with only negatively charged PEG (HS-PEG-COOH). This is in contrast to previous assembly studies of plant virus Au-VLPs.[29]

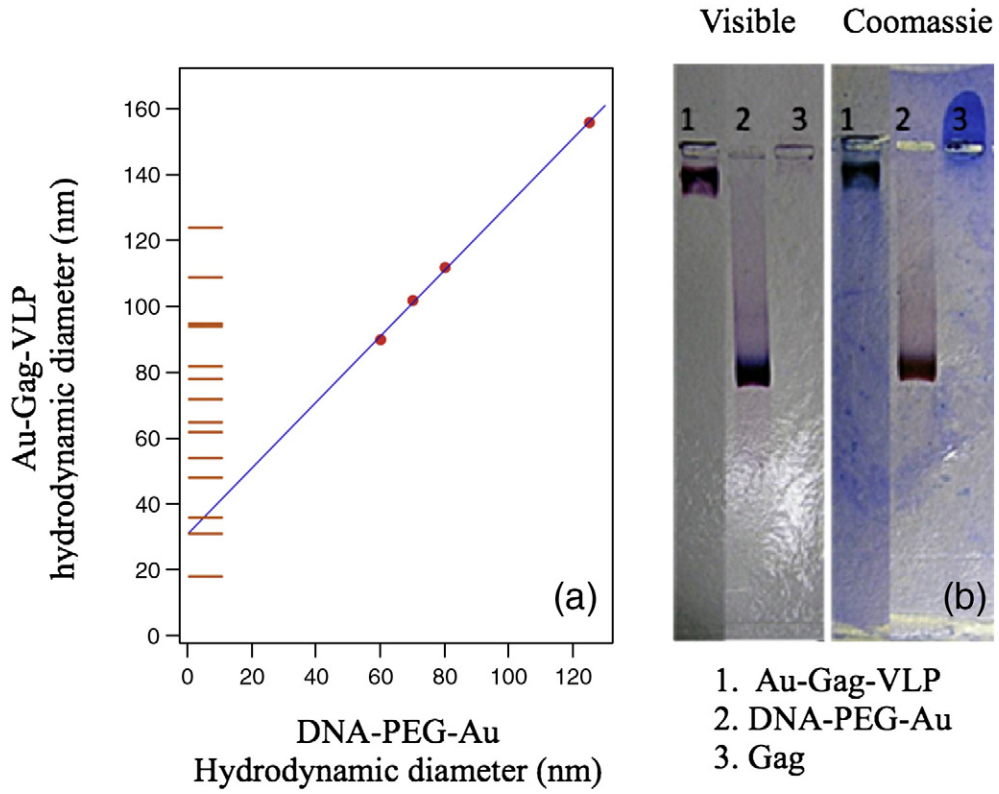

Fig. 1. (a) Hydrodynamic diameters of Au-Gag VLPs shown as a function of the hydrodynamic radius of DNA-coated gold nanoparticles (see Supporting Information, Fig. S3 for individual DLS values reported for each assembly). Horizontal lines along ordinate represent diameter values corresponding to successive *T*-numbers between $T = 1$ and $T = 48$. (b) Difference in electrophoretic mobility of DNA-functionalized gold before and after encapsulation within the Gag shell. Gag protein was added to DNA-PEG-Au particles, and an aliquot of the resulting suspension was stained with Coomassie blue. The suspensions were then electrophoresed through a 0.6% agarose gel: lane 1, DNA-PEG-Au particles with Gag; lane 2, DNA-PEG-Au particles alone; lane 3, Gag alone. The figure shows unstained (red color due to gold nanoparticles) and stained (showing protein) portions of each suspension.

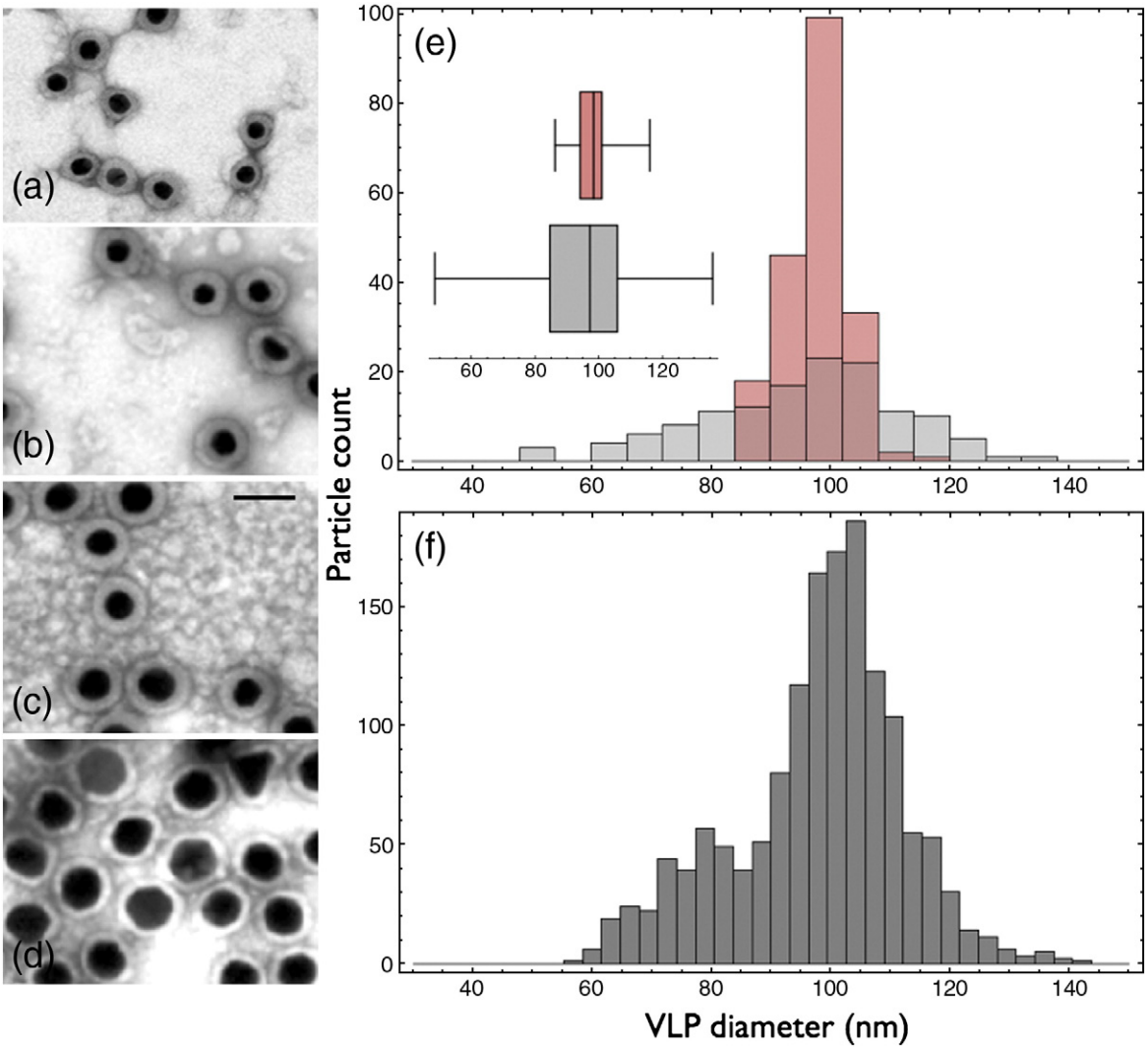

Fig. 2. (a–d) TEM micrographs of Au-Gag VLPs assembled using four different gold core diameters: 40 nm (a), 50 nm (b), 60 nm (c), and 80 nm (d). The scale bar represents 100 nm. (e) Comparison between histograms of diameters of Au-Gag VLPs (pink) encapsulating 60-nm cores and *in vitro* assembled Gag VLPs (gray). Inset: box and whisker plots for the two distributions. (f) Histogram of TEM-measured diameters of intact Au-Gag VLP particles assembled from an equal mixture of different diameter cores. The ratio of Gag molecules to cores was 15,000:1. There is a preferred VLP diameter at ~100 nm, corresponding to a 60-nm core.

Measurements of single Gag VLP diameters as a function of core size were performed by negative-stain electron microscopy (EM) (Fig. 2). EM Au-Gag VLP measurements confirmed the trend of the average Au-Gag VLP size found by DLS. However, distinct morphological differences were observed (Fig. 2a–d). Thus, assembly with 40-nm gold particles led to irregular deposition of Gag proteins, resulting in a variable thickness of the protein coat (Fig. 2a). In this case, most gold particles looked eccentrically placed with respect to the Gag shell. The average diameter of these Au-Gag VLPs was 81.3 nm with an SD of 8.6 nm. When 50-nm gold particles were used, the protein coat was more homogeneous than for smaller diameter gold nanoparticles (Fig. 2b). However, some particles had a partial but significant protein layer overlapping, which introduced some degree of ellipticity. The average diameter was 90.7 nm with an SD of 6.6 nm. Qualitatively, most of the variance in this case originates from the partial overlapping. When a 60-nm gold was used as a template, the vast majority of the particles were spherical and with a more uniform protein coating than for the smaller diameter gold nanoparticles (Fig. 2c). The degree of overlapping between protein layers persisted but appeared reduced relative to the case of the 50-nm gold cores. Furthermore, the smallest size variation was obtained: ±5.5 nm for a diameter of 100.7 nm. In the case of 80-nm gold cores (Fig. 2d), the assembly

reaction yielded roughly spherical particles, but the protein coat had a nonuniform appearance that suggests the presence of multiple defects. The average Au-Gag VLP diameter in this case was 115 ± 15 nm. The protein shell seems somewhat thinner on the 80-nm cores; however, because of the limitations of the negative-stain microscopy, it is difficult to ascertain whether this was a sample preparation artifact or a different shell morphology that may be associated with large cores.

We compared the size distribution of Au-Gag VLPs to that of a control assembly preparation in which Gag and PEG-DNA were mixed in solution, using identical conditions with the assembly of DNA-PEG-Au conjugates. A direct comparison of size histograms for Au-Gag VLPs (with core diameters of 60 nm) and free PEG-DNA VLPs in solution indicated that the 60-nm gold core reduced polydispersity by a factor of 4 as compared to free DNA in solution (Fig. 2e).

Thus, the EM analysis of Au-Gag VLPs obtained from different gold cores revealed that the 60-nm nanoparticles were the most suitable scaffolds for protein assembly, giving the most homogeneous Au-Gag VLPs. Notably, they had diameters similar to those of authentic immature HIV particles and *in vitro* assembled Gag particles.[7,18,19] This supports the idea that the natural packing of the Gag proteins preferred a core of 60 nm. To further explore the relationship between core diameter and particle assembly, we added Gag to a mixture containing equal numbers of gold nanoparticles of all the sizes studied. Enough Gag was added to coat all the nanoparticles. We then measured the diameters of the intact Au-Gag VLPs that were assembled. A histogram of these diameters is shown in Fig. 2f and

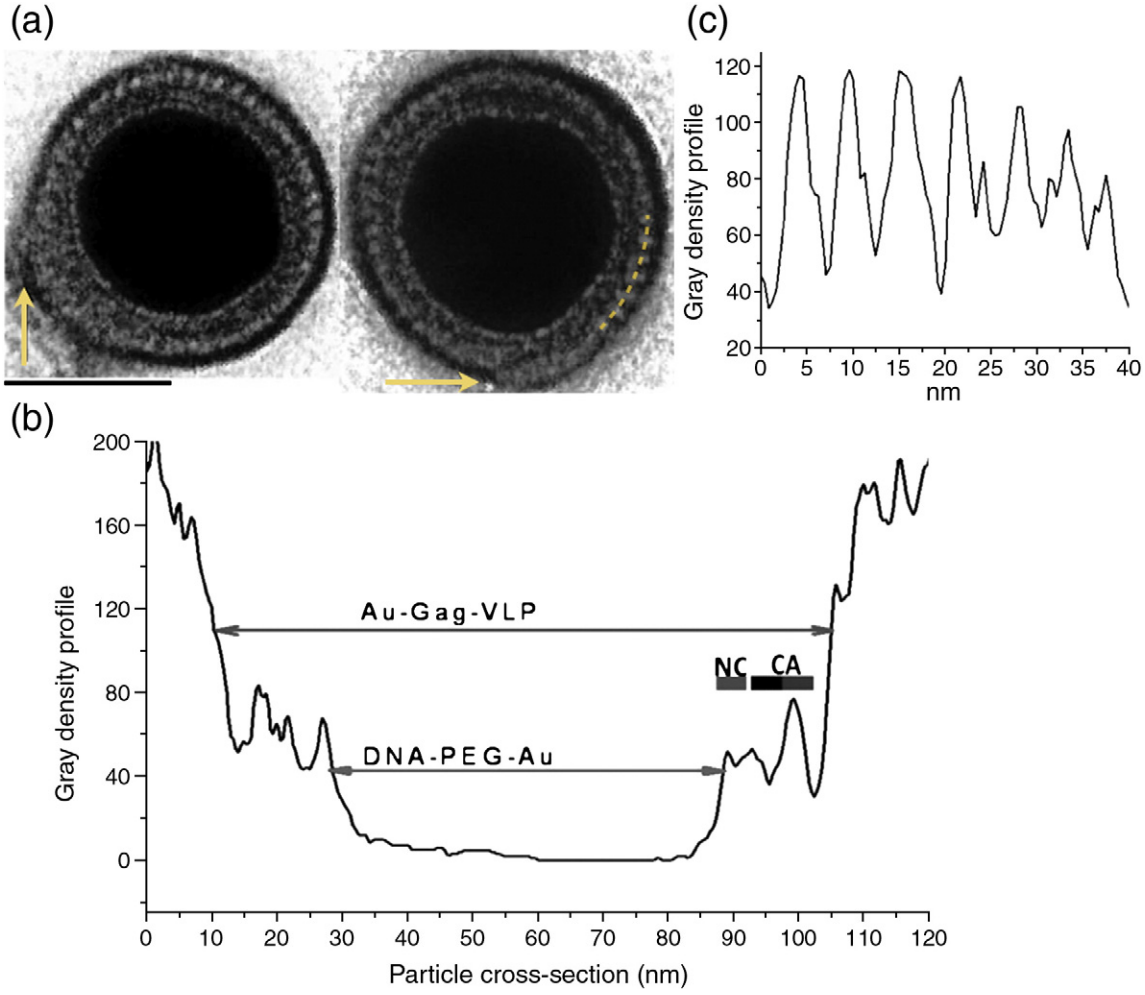

Fig. 3. Morphological features of single Au-Gag VLPs. (a) Two individual 60-nm gold particles encapsulated in Gag shells. The presence of the scar (arrows) was observed in most particles. The scale bar represents 50 nm. (b) Radial density distribution of a single Au-Gag VLP assembled on a 60-nm core. Stain density profile variations are consistent with the known sizes of different protein domains in Gag. (c) Density variation along the perimeter of a single Au-Gag VLP assembled on a 60-nm core [the density profile corresponds to the yellow circular arc of radius 48 nm depicted in (a)].

clearly indicates a preferred size for Au-Gag VLPs at ~100 nm, reflecting the fact that assembly on a 60-nm template is more likely to lead to an intact Au-Gag VLP than assembly on particles of other sizes. During templated assembly, not all assembling particles go to completion, that is, form a complete protein shell around the template. The 60-nm particles display a >80% completion efficiency under these assembly conditions, as visualized by negative-stain EM. This value is likely an overestimate since some incomplete particles could appear complete depending on their orientation. Regardless of the exact maximum efficiency value, Fig. 2f suggests that different core sizes have different encapsulation efficiencies.

More detailed morphological characteristics of the arrangement of Gag protein shell encapsulating the 60-nm core can be observed in Fig. 3a. The assembled shells had a striated pattern, with a spacing of ~4 nm between striations, as previously observed in Gag VLPs and immature HIV-1 particles.[18,19,34] However, to reveal the striated pattern, the stain had to be left in contact with the virus sample for 100 s instead of the more typical 10 s to allow stain penetration in the gaps between protein domains (Fig. 3a).

From previous work, *in vitro* assembled Gag subunits are expected to behave as radially oriented rods forming a spherical particle.[18,22] Au-Gag VLP morphology exhibited a similar arrangement corresponding to a monolayer protein coat (Fig. 3a). However, a small region reminiscent of a scar or an overlap of two protein layers was clearly visible and, interestingly, was present in all particles. This novel feature may be attributed to a local stitching mismatch due to a mechanism of Au-Gag VLP formation involving proteins being added to the growth edge during assembly or, as discussed below, it could be the result of the influence of the Gag anisotropy combined with spherical template constraints.

A cross-section analysis of the negatively stained single particles revealed densities that could be attributed to the three structural domains of the recombinant Δ16–99 Gag, namely, the N- and C-terminal domains of CA and the NC portions of Gag (Fig. 3b). This assignment of the stain density peaks is consistent with the known protein density profile for *in vitro* assembled Gag.[7,18,22] The thickness of the protein shell, corresponding to the length of Gag in these particles, was ~15 nm, consistent with values obtained from DLS analysis. In addition, the spatial period of the striation pattern of ~4–5 nm near the circumference of the particle was consistent with the spacing previously observed in cryoelectron microscopic tomograms of immature HIV particles[7,18,19,34] (Fig. 3c).

The apparent uniformity of Au-Gag VLPs with 60-nm cores permitted further electron micrograph data processing through three-dimensional (3D) particle reconstruction.[35] Virus particles were imaged under negative-stain conditions and then classified and averaged, as described in Materials and Methods. The final model (Fig. 4) was constructed from 5000 particles with no preimposed symmetry. The final averaged reconstruction revealed the scar region in more detail. It appears that the scar represents an extended defect occupying approximately half of the great circle and having an area equal to ~30% of the total VLP surface area. It is not clear whether the scar is the result of an overlapping between the two edges of the same layer or if there is a partial extra layer acting like a patch covering a gap.

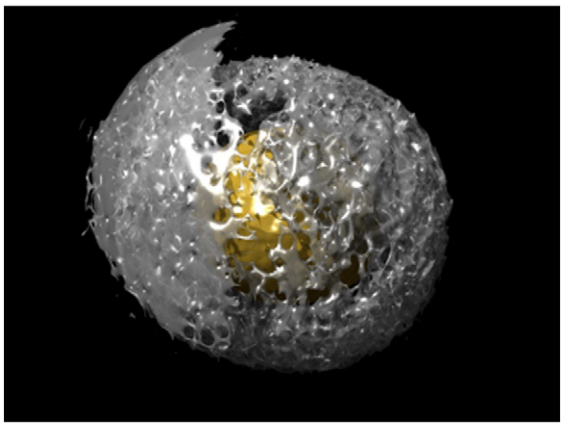

Fig. 4. Single-particle reconstruction of *in vitro* assembled Au-Gag VLPs at 62 Å resolution. The recombinant Gag protein (gray) self-assembles in two incomplete spherical regions around the 60-nm-diameter gold nanoparticle (yellow). The class averages used for the generation of this model are consistent with the protein arrangement seen in TEM indicating the existence of an extended scar-like defect.

The model resolution in Fig. 4 was ≈62 Å (see Fig. S4). This is insufficient for the identification of any of the postulated hexameric arrangements within the protein shell. Nevertheless, 120° angles can be frequently observed throughout the surface protrusion network. The presence of a spherical core at the center of the particle was not believed to interfere with the reconstruction, since similar VLP reconstructions of native structures encapsulating nanoparticles have been already reported.[29,33] The low resolution is attributed to the absence of symmetry constraints and the presence of the extended defect, which made it difficult to achieve convergence with a higher degree of fidelity. However, even at this resolution, surface morphology is not completely isotropic. Figure 5a highlights the existence of the scar as the boundary between two different isodensity regions (colored differently). Figure 5b provides a schematic of a half-shell wrapping

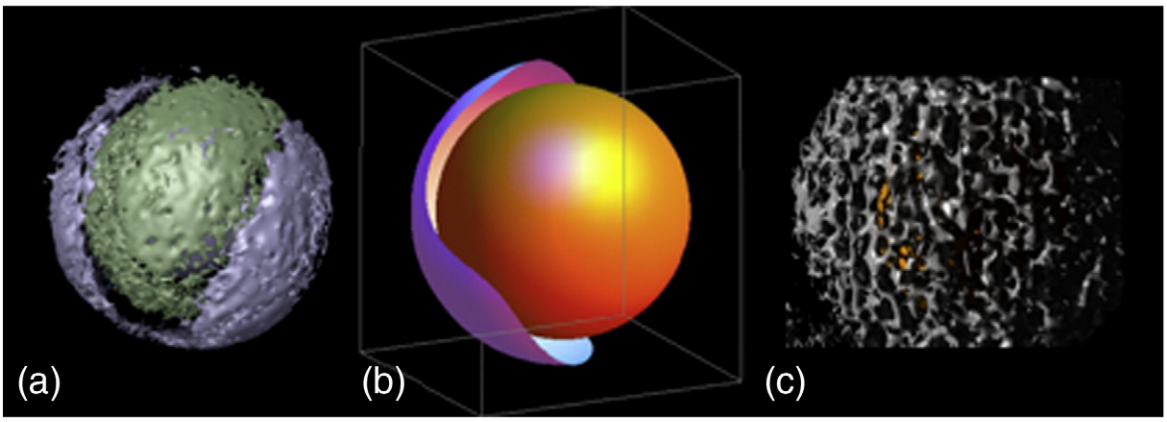

Fig. 5. Reconstructed Au-Gag VLP morphology. (a) Single-particle reconstruction model of Au-Gag VLP highlighting the division of the particle surface into large, partially disconnected regions (colored differently). (b) Cartoon showing a spherical patch covering approximately half of the surface of a sphere—internal assembly constraints may play a role in the size of the patch and dictate the shape of the edges. (c) Close-up of an area from (a). A unidirectional pattern of ridges (oriented vertically in the figure) can be observed, as expected for rod-like structures arranged on the surface of a sphere.

around a spherical template. There is space on the surface for another half-shell to form. Figure 5c shows a close-up of an area of Fig. 5a where one can notice a regular array of ridges (of vertical orientation in the picture) under grazing model illumination. The ridges are oriented approximately at 45° to the direction of the scar defect.

We also examined "conventional" VLPs, assembled from Gag and yeast tRNA in solution. Interestingly, a discontinuity or even two are also visible in many of these particles (see Fig. S5).

Quantification of Gag surface coverage

The number of protein subunits reported for the average immature HIV particle has been previously estimated at ~5000 by cryoEM, assuming a complete, hexagonally packed protein shell.[5,34] However, recent structural analysis of immature particles by cryoelectron tomography suggested that the Gag lattice is incomplete and accounts for only ~50% of the particle.[18,19,24] Based on these observations, each immature particle should contain ~2500 copies of Gag. However, visible variations in the protein content and size of immature HIV particles make the measurements challenging, and these numbers are only approximate.

Au-Gag VLPs are more uniform than immature HIV particles, and therefore, measurements of their stoichiometry should be more straightforward. The spacing between striations in Fig. 3 is consistent with the reported HIV inter-hexamer distance (5–8 nm apart) within the unit cell of a hexameric lattice.[7,18,19,34] Therefore, the estimated number of Gag monomers in this work is consistent with the predicted Gag stoichiometry of *in vitro* assembled Gag VLPs assuming a complete Gag lattice.[18,34] However, since this estimate relies on a microscopic method, an ensemble-averaging complementary approach was needed to test its validity. UV-Vis and fluorescence spectroscopy were used for this purpose. Thus, after assembling gold nanoparticles with Δ16–99 Gag in 0.1 M NaCl buffer and removal of excess protein by dialysis (using a dialysis membrane with a 500-kDa cutoff pore size), the VLPs were disassembled by dialyzing against 0.5 M NaCl buffer (see Fig. S2). The released protein and Au templates were followed back into solution and were quantified by UV-Vis and fluorescence spectroscopy. There were marked differences between the tryptophan emission spectra when Gag was part of the shell (assembled VLP) or free in solution (disassembled VLP) (Fig. S6a). Native tryptophan fluorescence is a well-established reporter for changes in the local chemical environment of the tryptophan. The emission peak for Au-Gag VLP has an apparent red-shift of ~90 nm with respect to free protein. At first sight, this is surprising since one would rather expect a blue shift due to a decrease in the polarity of Trp environment upon assembly[36] However, the Au particle has a distance-dependent fluorescence quenching effect; therefore, Trp residues close to the Au surface will be absent from the emission spectrum.[37] In contrast, externally placed Trp residues will be less affected by the quenching. As they will be in contact with polar water molecules, they will be red-shifted. This explains the persistence of common red-shifted bands between free and bound protein samples. As there is no emission peak at 324 nm from the Au-Gag VLPs, this peak is a good reporter of the level of free Gag in solution.

The completeness of the disassembly process was monitored through UV-Vis spectroscopy (Fig. 6)

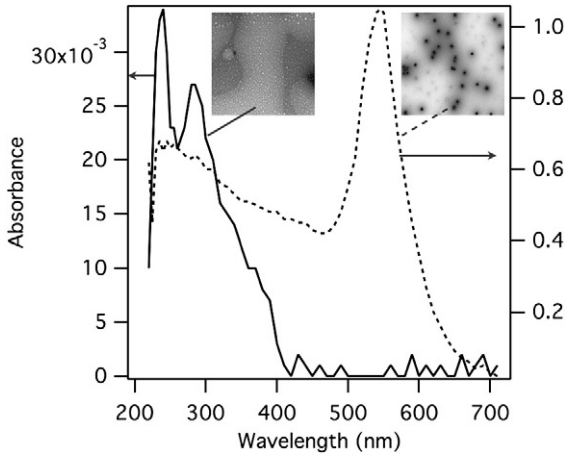

Fig. 6. Au-Gag VLP disassembly followed by UV-Vis spectroscopy and TEM. The absorbance profile of recombinant Gag assembled on the surface of 60-nm gold nanoparticles (dash curve) shows a plasmon band at 548 nm corresponding to gold. A broad band at 280 nm corresponds to protein. Absorbance measurements from disassembled Gag show only the band corresponding to protein at 280 nm (continuous line). TEM images of Au-Gag VLPs (right EM image) subjected to disassembly dialysis show the liberation of Gag from the nanoparticles into solution (left EM image).

and TEM (inset, Fig. 6). Negative-stain TEM shows the Au-Gag VLPs before disassembly (inset on the right) but could not detect any protein remaining on the cores after the disassembly and separation procedures (left). The absorbance profile of the Au-Gag VLPs (dashed curve) shows a band at 548 nm, corresponding to gold, in addition to the band at 280 nm, corresponding to the protein. The plasmon peak for a naked spherical gold nanoparticle of 60 nm is expected to occur at 538 nm; however, the plasmon peak is red-shifted by 10 nm in the presence of the nucleic acid and protein coat. The characteristic surface plasmon peak of the gold nanoparticle cores after disassembly was indistinguishable from the surface plasmon peak of core particles before assembly (not shown). The absorbance profile of disassembled VLPs, after removal of the gold nanoparticles, shows only the band corresponding to the Gag protein (continuous line); the intensity of the absorbance band at 280 nm, corresponding to protein, is lower than Gag absorbance within the shell due to dilution of the Au-Gag VLP sample during dialysis (Fig. S2).

The number of Gag proteins per gold nanoparticle was then determined from fluorescence of samples containing disassembled Gag (Fig. S6). Tryptophan emission was measured for a set of four preparations, and the corresponding protein concentration was calculated from a Δ16–99 Gag calibration curve (Fig. S6b). In addition, the protein concentration in the disassembly reactions was also determined from the Bradford assay. The absorbance of four samples containing Coomassie blue dye was measured, and the concentration was calculated from a calibration curve of recombinant Gag (Fig. S6c).

The number of Gag molecules within an Au-Gag VLP was then estimated by dividing the Gag concentration by the gold nanoparticle concentration in each preparation, measured prior to disassembly. As shown in Fig. S6d, the average Gag protein number per particle was 4490 ± 490 from absorbance and was 4880 ± 288 from fluorescence. Notably, the two techniques agree well, and the results are in excellent agreement with the previously estimated Gag stoichiometry corresponding to complete VLPs of immature HIV-1.[18,34]

Discussion

One way to pack identical protein subunits onto a spherical surface is according to the quasi-equivalence principle. Many quasi-equivalent virus shells, and VLPs formed from the capsid proteins of icosahedral viruses, exhibit a linear correlation between the charge on the internal surface of the capsid and the size of the nucleic acid;[38] however, their diameters are restricted because of the discrete nature of their *T*-numbers. In contrast, immature retroviral particles produced *in vivo*,[7] as well as VLPs assembled on nucleic acid *in vitro*, possess a wide range of diameters. Similarly, Au-Gag VLPs containing a gold template form with any diameter within a range between 80 nm and 160 nm, with a median diameter of ~100–120 nm. These Au-Gag VLPs are unlikely to obey the quasi-equivalence principles of icosahedral protein shells and must follow a different principle for spherical packing of identical subunits. Nevertheless, we found that the efficiency of assembly is biased toward shells with a diameter of approximately 100 nm, encapsulating a core of 60 nm diameter coated with approximately 2000 fifty-base ss-DNA molecules (Fig. 2; see Materials and Methods for details on DNA quantification and references). The number of Gags per gold particle found (i.e., 5000) is roughly consistent with a protein dimer interacting with an ss-DNA molecule. As the Gag NC domain (residues 377–431) contains a net positive charge of 11, ~55% of the internal capsid interfacial charge is neutralized by the core. Since no strict *T*-number constraints are likely to exist, the variations in the assembly efficiency in Fig. 2 are probably coming from the protein–core interaction. For icosahedral ss-RNA viruses, such core-size selectivity has been qualitatively explained by the interplay between capsomer–capsomer and capsomer–genomic cargo interaction energies, which reached a minimum corresponding to the partial neutralization of interfacial charges.[39] However, for

the HIV-Gag case, the template–protein subunit interactions leading to assembly specifically require nucleic acid. This may be because the maximum surface charge coverage obtainable with PEG-DNA is more than twice the maximum surface charge attainable with PEG-COOH-modified templates. Other virus capsid proteins require specific genomic sequences for assembly,[28] but they also form capsids with well-defined *T*-numbers. Therefore, one intriguing feature of HIV-Gag is that, despite its cargo-protein shell specific interactions, its architecture does not follow the quasi-equivalence rules even when the assembly is constrained by a rigid spherical nanoparticle template.

The absence of global symmetry, despite local symmetry, implies the presence of lattice defects. Indeed, Au-Gag VLPs exhibit an extended defect that occupies a large continuous area of the shell (Fig. 4). Our reconstructed model of Au-Gag VLPs encapsulating 60-nm-diameter cores suggests that the defect is similar to a seam and may involve either an area of overlap between a secondary protein lattice that patches a vast empty region left by the primary lattice, or an overlap of the edges of the same lattice. The presence of the same type of defect in all particles is especially intriguing and suggests that the extended defect configuration is likely to correspond to a free-energy minimum for spherical packing. The question is then, under what conditions does a surface spherical packing of subunits yield such an extended defect or a system of defects that will form a stable scar? A possible answer to this question requires a brief consideration of theoretical works on spherical packing modeling of virus shells.

In a spherical disk-packing approach to virus assembly, Bruinsma *et al.* have shown that, for the icosahedral symmetry to correspond to a free-energy minimum, the existence of a conformational switch is required.[40] For completely identical subunits (e.g., hexamers), icosahedral symmetry does not correspond to a minimum, and a multitude of local free-energy minima exist corresponding to a variety of defects. Experimental observations corresponding to these predictions were made by Chang *et al.*[41] In their studies, cowpea chlorotic mottle virus capsid proteins were assembled upon anionic-surfactant-coated oil-in-water nanoemulsion droplets. The resulting VLP shells exhibited an apparently continuous range of diameters, each characterized by different kinds of defects and disorder. In an earlier work, Sorger *et al.* described self-assembled turnip crinkle virus structures involving partial overlap of icosahedral shells.[42] These "monster particles" were discussed 20 years later in a computer simulation paper from Nguyen *et al.*[43] and then, still more recently, in theoretical work by Levandovsky and Zandi on "seams" arising in cone-like mature HIV capsids.[44] However, in contrast with the early observations of Sorger *et al.* concerning turnip crinkle virus where the occurrence of overlapping defects were rare (few percent), what is intriguing for the Au-Gag VLPs in the present study is that most particles appear to have the same kind of defect.

Bausch *et al.*[45] have considered the problem of the ground state for packing of small spherical subunits on the surface of a greater sphere. Similar to disks, a triangular lattice of spherical subunits cannot be wrapped on the curved surface of a sphere; defects or variation in coordination number must exist. The departure of the coordination number from the preferred planar value of 6 is termed disclination charge. Bausch *et al.* have proposed that, at large radii of the spherical template, isolated disclination charge defects would induce too much strain. This excess strain could be relieved by introducing dislocations, which consist of pairs of tightly bound coordination defects linked together, forming grain boundary scars. Experiments by the same group, with micrometer-size beads assembled on the surface of water droplets in oil confirmed indeed the existence of scar defects across a triangular lattice not found in planar crystals.[45] The elongated defect observed in Au-Gag VLPs in our present work could be the result of grain boundary scar formation. However, it is not clear why there should be a single scar spanning the entire particle.

One property that distinguishes the Gag subunit from a disk or a sphere is its aspect ratio: Gag subunits are better described as rods with an aspect ratio of ~6–8.[6,7,18,19] Moreover, the Gag subunit length represents a significant fraction (~50%) of the radius of curvature of a 60-nm Au core. On a flat template, such rod-like molecules will assemble in a parallel configuration, not unlike the packing in a liquid crystal state. However, parallel orientation and spherical templating are conflicting constraints. When anisotropic subunits are forced into spherical packing by a template, a two-dimensional liquid crystal phase will appear on the surface. For rods lying flat on a spherical surface, Nelson suggested that spherical topology will force a number of disclination defects in the ground state,[46] resulting in a stable surface packing with one seam having a pattern reminiscent of that on a baseball cover. The high aspect ratio of the assembling subunits in this case induces one long boundary between two domains, each covering half of the spherical template.

To the best of our knowledge, the problem of rod-like subunits bound to a spherical surface at one end and constrained to assemble by lateral interactions has not been approached yet. However, self-organization is known to occur in similar systems, albeit at different spatial scales. For example, Luedtke and Landman[47] have described the organization of self-assembled linear alkanethiols in domains of equal size separated by continuous bare areas on gold spherical cluster surfaces when

the radius of curvature of the template was comparable with the ligand length. In another study, Kuna *et al.* reviewed self-organization in blends of immiscible molecules. Such mixtures separate into domains of well-defined shape and size on the surface of spherical templates, but not on planar substrates.[48]

The single-particle reconstruction model of Au-Gag VLPs revealed features that are consistent with a boundary running across the entire particle and separating its surface into two distinct areas. (Fig. 5a). This boundary could be the result of two mismatched crystalline phases coming together. The relative consistency of the shape of this boundary from one particle to another could be the signature of a rod-like subunit organization. It is possible that these two areas are the result of independent growth processes. Thus, after a surface nucleation process, the growth of a hexagonal lattice could occur with the strain due to curvature being relieved at the growing edge. Strain energy will increase with the size of the system.[45] When the rate of change in strain energy equals the rate of free-energy decrease from protein association, growth stops. In the meanwhile, the bare area still available (Fig. 5b) could host the formation of a new layer; when the second layer meets the first, it might stop or overlap slightly with it. Template-induced stress would be relieved at this boundary. The anisotropic ridge structure in Fig. 5c is consistent with the existence of a phase characterized by orientational order (similar to liquid crystals). In conclusion, it is possible that a significant subunit aspect ratio and length relative to core radius represent factors that could lead, in principle, to the observed stable morphology involving a boundary between extended areas harboring liquid crystal order.

How might the factor of length-to-particle radius ratio contribute to some of the observed properties of native immature HIV-1 particles? One possibility is that, as previously reported,[18,19,24] authentic particles contain sizable gaps in the Gag lattice. Perhaps, as suggested,[24] the discontinuities in the lattice, which are unavoidable consequences of the geometric constraints of high aspect ratio and length of the Gag subunits, provide access for the endosomal sorting complex required for transport (ESCRT) machinery,[49] leading to release of the particle before assembly of the Gag shell is completed. However, it is also possible that authentic particles are more complete than they appear. For example, liquid crystalline states of different local order may require special attention during cryoTEM data interpretation. Thus, if such regions of different continuous orientational order existed in the immature HIV-1 virions, one would expect that they would have different electron diffraction properties. In turn, this might affect their appearance in cryoTEM images and could contribute to underestimation of the completeness of the Gag lattice. In fact, there is a striking similarity between the half-baseball-shaped Au-Gag VLP shell in Fig. 5 and the immature lattice maps in Fig. 2c of Briggs *et al.*[18] We suggest that the growth modes of immature HIV-1 viruses and Au-Gag VLPs must be similar, with the strain increasing as the hexagonal lattice, with its accompanying spherical constraint, grows. In the case of immature HIV particles, this constraint could come from the interaction between the nucleic acid and Gag. In the case of Au-Gag VLPs, it is also imposed by the curvature of the template. In authentic particles, the growth stops or slows down when the strain balances the gain in free energy due to assembly. However, in the case of Au-Gag VLPs, the remaining exposed Au-DNA area acts as a template for starting the process over and growing another sheet of Gag, which explains why Au-Gag VLPs are characterized by connected Gag coverage. Assembly on RNA may occur in a similar fashion: electron microscopic images of *in vitro* assembled particles show shell discontinuities and coverage reminiscent of those observed for Au-Gag VLPs (Supporting Information, Fig. S5). However, the sequential nature of particle growth may allow authentic immature HIV particles to be released from mammalian cells before the shell is complete. It should also be noted that authentic particles, as well as VLPs assembled *in vitro*, can be formed using several or many RNA molecules,[50] while the Au-Gag VLPs are formed around a homogeneous core and an excess of nucleic acid; the use of multiple RNA molecules might also contribute to the "facets" described by Fuller *et al.*[6]

Conclusion

In summary, evidence is provided for a significant decrease in the polydispersity of self-assembled HIV-1 Gag protein particles when Gag protein self-assembly is promoted with a DNA-coated metal nanoparticle template. The proposed template-directed experimental model for HIV-1 immature particles is consistent with a complete Gag lattice having approximately 5000 protein subunits bound to an average of 10^5 nucleotides of DNA on each particle. 3D EM single-particle reconstruction indicates the presence of an extended defect in the protein shell corresponding to a scar that separates the particle into two approximately equal parts. The close packing of anisotropic Gag subunits combined with the existence of strong spherical core/shell interactions raise the question of a possible liquid crystal phase behavior of the Gag lattice that could be the origin of the observed scar and anisotropy.

The novel feature of the present work was the use of a homogenous nanoparticle "template" upon which the Gag lattices were assembled. This

significantly reduced the variability of the resulting particles and can therefore facilitate the analysis of the lattice. We believe that this approach will be useful in unraveling the structural features of retrovirus particles. The opaque Au particles we have used here are incompatible with cryoEM, but we have recently succeeded in assembling HIV-1 Gag lattices using transparent nanoparticles, and we are now performing tomographic analysis of these VLPs.

Materials and Methods

Materials

Citrate-coated gold nanoparticles (40 nm, 50 nm, 60 nm, and 80 nm) were purchased from Ted Pella (Redding, CA). Thiol-modified oligonucleotides were purchased from Integrated DNA Technologies, Inc. (Coralville, IA) {5′ HS-3[$(CH_2CH_2O)_6$ phosphoramidite]-$(TG)_{25}$ 3′}. NAP-25 columns (Sephadex G-25 DNA grade) were purchased from GE Healthcare (Piscataway, NJ). Slide-A-Lyzer mini dialysis unit 20K molecular weight cutoff (MWCO), 10K MWCO, and dithiothreitol (DTT) were purchased from Pierce Biotechnology, Inc. (Rockford, IL). Hepes and sodium chloride were purchased from Sigma-Aldrich. Float-A-Lyzer micro dialysis unit 100KD was purchased from Spectrum Laboratories, Inc. (Rancho Dominguez, CA). Nanosep centrifugal devices 300K MWCO were purchased from Pall Life Sciences (Ann Arbor, MI). Four hundred mesh carbon-coated Cu grids were purchased from Electron Microscopy Sciences (Hatfield, PA). Bradford assay kit was purchased from Pierce Biotechnology, Inc. Eppendorf UVette was purchased from Eppendorf (Westbury, NY). MilliQ water (>18.0 MΩ) was used for all experiments.

Imaging and spectrophotometry

Absorbance measurements of gold nanoparticles were taken using NanoDrop ND-1000 UV-Vis spectrophotometer. To prevent saturation, we used 10× diluted aliquots of the master colloidal solutions for analysis. The plasmon bands of the differently sized particles (40–80 nm) were between 530 nm and 545 nm, as expected. The gold concentration in assembly reactions was measured without dilution. The absorbance maximum was observed at 550 nm for 60-nm gold. Bradford assay to determine protein concentration was performed in a UV-Vis absorption spectrometer (Eppendorf BioPhotometer) using Eppendorf UVettes (2 mm path length). Fluorescence measurements were performed on a PerkinElmer fluorometer (model LS50B) using a low-volume quartz cuvette. TEM data were recorded on a JEOL 1010 equipped with a 4 k CCD camera, operating at 80 kV. Negatively stained electron micrographs of gold nanoparticles and Au-Gag VLPs were prepared by placing the grid on top of a sample droplet for 4 min. After wicking out the excess solution, the grid was placed on top of a water droplet for 20 s and wicked again. Finally, the grid was placed on top of a 1% uranyl acetate solution for 1 min, and excess solution was removed with filter paper. Au-Gag VLP diameters and efficiencies were determined using two or more grids independently prepared, with at least 800 particles imaged per grid. DLS (Zetasizer Nano-S; Malvern) of assembly reactions was performed to determine the hydrodynamic size increase after protein attachment on the nanoparticle (Fig. S3). Prior to DLS measurements, all solutions were filtered using a 0.2-μm syringe filter to remove large aggregates that would otherwise dominate the scattering. The hydrodynamic radii of the particles were calculated after 20 runs for each measurement, taken at 4 °C.

Synthesis of DNA-PEG-Au

Functionalization of citrate-coated gold with 5′ thiol-modified PEG-DNA oligonucleotides {5′ HS-3 [$(CH_2CH_2O)_6$ phosphoramidite]-$(TG)_{25}$ 3′} was carried out with a slight modification of the protocol of Hurst *et al.*[51] Briefly, freshly reduced disulfide bonds at the 5′ end of the nucleotides were added in excess to the gold nanoparticles by mixing citrate-coated gold (10 ml, ~10^{13} particles/cm^3, from stock bottle) and DNA (2 mg). After 2 h of incubation, the mixture was brought to 0.01 M in phosphate buffer (pH 8) and 0.01% in SDS. After another 90 min of incubation, the mixture was brought to 0.05 M NaCl in phosphate buffer and then 0.1 M followed by sonication for 10 s. The ionic strength was subsequently increased to 1 M at 0.1-M intervals and spaced every 15 min. Thereafter, the reaction was incubated for 2 days at room temperature in order to ensure the oligonucleotide saturation on the nanoparticle surface. The excess oligonucleotide was removed through centrifugation (38,000*g*, 40 min, and 4 °C; floor model preparative ultracentrifuge, type 50.2Ti rotor, Beckman). Pelleted DNA-PEG-Au conjugates were resuspended in high ionic strength buffer [50 mM Hepes and 0.5 M NaCl (pH 7.5)] and washed for a total of 5× to remove excess DNA. The final pellet was resuspended and stored in water. In total, four DNA-PEG-Au conjugates were synthesized, differing only in the nanoparticle diameter (40 nm, 50 nm, 60 nm, and 80 nm).

The number of ss-DNA bound to 60-nm Au cores was estimated by previously established methods using similar fluorescently labeled thiol PEG-DNA molecules. The concentration of DNA was determined from fluorescence data after detaching the DNA molecules from the nanoparticle surface.[51,52]

Assembly of Δ16–99 Gag around DNA-coated gold nanoparticles

Encapsulation of DNA-PEG-Au particles inside recombinant Gag was carried out by adapting the Datta *et al.* protocol.[21] The recombinant protein, Δ16–99 Gag, was prepared according to published protocols.[21,53] The solubility of the protein was enhanced by eliminating the myristate modification. The protein also lacked the p6 domain.[20,54]

Typically, *in vitro* assembly of Δ16–99 Gag was induced at a number ratio of 15,000 equivalent Gag to 1 gold nanoparticle. The concentration of gold particles was calculated from its absorbance value at 450 nm and the

molar extinction coefficient related to the particle size.[55] Prior to mixing with Δ16–99 Gag, DNA-PEG-Au in water was buffer exchanged with high ionic strength buffer [50 mM Hepes and 0.5 M NaCl (pH 7.5)] at room temperature and was mixed with the corresponding amount of concentrated recombinant Gag in storage buffer [50 mM Hepes, 0.5 M NaCl, and 4 mM DTT (pH 7.5)]. The mixture was diluted with high ionic strength buffer to a final protein concentration of 1 mg/ml. The assembly reaction was dialyzed (20K MWCO) overnight against low ionic strength buffer [50 mM Hepes, 0.1 M NaCl, and 1 mM DTT (pH 8.0)] at 4 °C. Next day, assembly products were recovered from the dialysis bag and were concentrated (300K MWCO, 7000*g*, 4 °C) for EM analysis or subjected to a second dialysis (100K MWCO) for removal of unbound Gag.

EM and 3D image reconstruction

Au-Gag VLPs in [0.1 M NaCl and 50 mM Hepes (pH 8)] at a concentration of 2.5 nM were stained with 1% uranyl acetate aqueous solution on freshly glow discharged carbon-coated copper grids (400 mesh; Electron Microscopy Sciences). The samples were viewed on JEOL 1010 operating at 80 kV and at an effective magnification of 30,000× for an effective 3.77 Å/pixel at the specimen level. Densitometric analysis of particle cross-sections was performed using IgorPro image processing software.

Image reconstruction was performed using the EMAN software suite v.1.8 for Linux. Particles were selected using EMAN.[56] In total, ~4900 particles were boxed, center aligned, and used for reconstruction. Class averages were generated, and low-noise class averages were used to generate an initial model. The particle data set was then refined with the initial model thus generated without assuming any symmetry. This was performed to avoid the possibility of initial model bias. The reconstructions were done from a model generated from the individual particles taken from the micrograph. Also, the Fourier shell transform (see Fig. S4) is the correlation of models generated from even and odd particles in the reconstructions. The final model converged to ~ 62 Å resolution as judged by $\sigma = 0.5$ on Fourier shell correlation (Fig. S4). The final model was visualized, and the 3D images were rendered using UCSF Chimera.

The efficiency of encapsulation was estimated as the number of intact VLPs (i.e., those composed of a continuous single layer of protein surrounding a single Au core) divided by the total number of gold nanoparticles in a micrograph. Thus, the total number of gold nanoparticles includes those that have formed intact VLPs (by eye) and those that have incomplete shells or are part of Au/protein aggregates. For the 60-nm cores, >80% of the particles were scored as intact.

Quantification of Δ16–99 HIV-1 Gag assembled on 60-nm gold nanoparticles

The number of Gag proteins loaded onto each particle was determined from the concentration of nanoparticles and the protein concentration corresponding to a completed Au-Gag VLP assembly reaction. Gold nanoparticle concentration after assembly was estimated from UV-Vis spectroscopy data, where the absorbance (A) at 450 nm ($\varepsilon = 1.57e10\ M^{-1}\ cm^{-1}$)[55] for each sample was related to the nanoparticle concentration through Beer's law.

To quantify the protein in each assembly, viral proteins were detached from the nanoparticle surface during an 18-h dialysis against high ionic strength buffer. Subsequent centrifugation (40,000*g*, 30 min, benchtop microcentrifuge) resulted in gold separation. The remaining supernatant, containing only free proteins, was employed for concentration measurements in each sample. The protein concentration was then estimated by two methods as described below.

To determine the protein concentration through quantitative tryptophan fluorescence, we placed 50 μl of supernatant in a quartz cuvette, and the tryptophan fluorescence ($\lambda_{excitation} = 290$ nm) was compared to a standard curve. Gag protein standards were prepared in the same buffer as the supernatant. Fluorescence emission was collected from 300 nm to 500 nm, with a fluorescence maximum peak observed at 324 nm (Fig. S6).

In addition, protein concentration in the supernatant was estimated from UV-Vis absorption spectroscopy. The Bradford assay directly relates the absorbance of Coomassie dye ($\lambda_{abs} = 595$ nm) to the protein present through the formation of a protein–Coomassie complex. Thus, the absorbance of the supernatant–dye complex was compared to a calibration curve. The protein used for the calibration curve was bovine serum albumin diluted in the same buffer as the supernatant (Fig. S6).

The number of Gag proteins per particle in each assembly reaction was calculated by dividing the concentration of Gag proteins by the concentration of nanoparticles. Protein quantification experiments were carried out in quadruplicate using fresh Au-Gag VLP samples each time.

Supplementary materials related to this article can be found online at doi:10.1016/j.jmb.2011.04.012

Acknowledgements

We gratefully acknowledge support from the National Science Foundation (grants 0832651 and 0708590) and the National Institutes of Health (grant GM081029). This work was also supported in part by the Intramural Research Program of the NIH, National Cancer Institute, Center for Cancer Research.

References

1. Benjamin, J., Ganser-Pornillos, B. K., Tivol, W. F., Sundquist, W. I. & Jensen, G. J. (2005). Three-dimensional structure of HIV-1 virus-like particles by electron cryotomography. *J. Mol. Biol.* **346**, 577–588.
2. Briggs, J. A., Wilk, T., Welker, R., Krausslich, H. G. & Fuller, S. D. (2003). Structural organization of authentic, mature HIV-1 virions and cores. *EMBO J.* **22**, 1707–1715.

3. Ganser-Pornillos, B. K., Cheng, A. & Yeager, M. (2007). Structure of full-length HIV-1 CA: a model for the mature capsid lattice. *Cell*, **131**, 70–79.
4. Pornillos, O., Ganser-Pornillos, B. K., Kelly, B. N., Hua, Y., Whitby, F. G., Stout, C. D. *et al.* (2009). X-ray structures of the hexameric building block of the HIV capsid. *Cell*, **137**, 1282–1292.
5. Ganser-Pornillos, B. K., Yeager, M. & Sundquist, W. I. (2008). The structural biology of HIV assembly. *Curr. Opin. Struct. Biol.* **18**, 203–217.
6. Fuller, S. D., Wilk, T., Gowen, B. E., Krausslich, H. G. & Vogt, V. M. (1997). Cryo-electron microscopy reveals ordered domains in the immature HIV-1 particle. *Curr. Biol.* **7**, 729–738.
7. Wilk, T., Gross, I., Gowen, B. E., Rutten, T., de Haas, F., Welker, R. *et al.* (2001). Organization of immature human immunodeficiency virus type 1. *J. Virol.* **75**, 759–771.
8. Salzwedel, K., Martin, D. E. & Sakalian, M. (2007). Maturation inhibitors: a new therapeutic class targets the virus structure. *AIDS Rev.* **9**, 162–172.
9. Sticht, J., Humbert, M., Findlow, S., Bodem, J., Muller, B., Dietrich, U. *et al.* (2005). A peptide inhibitor of HIV-1 assembly *in vitro*. *Nat. Struct. Mol. Biol.* **12**, 671–677.
10. Zhang, H., Zhao, Q., Bhattacharya, S., Waheed, A. A., Tong, X., Hong, A. *et al.* (2008). A cell-penetrating helical peptide as a potential HIV-1 inhibitor. *J. Mol. Biol.* **378**, 565–580.
11. Amarasinghe, G. K., De Guzman, R. N., Turner, R. B., Chancellor, K. J., Wu, Z. R. & Summers, M. F. (2000). NMR structure of the HIV-1 nucleocapsid protein bound to stem–loop SL2 of the ψ-RNA packaging signal. Implications for genome recognition. *J. Mol. Biol.* **301**, 491–511.
12. De Guzman, R. N., Wu, Z. R., Stalling, C. C., Pappalardo, L., Borer, P. N. & Summers, M. F. (1998). Structure of the HIV-1 nucleocapsid protein bound to the SL3 ψ-RNA recognition element. *Science*, **279**, 384–388.
13. Gamble, T. R., Vajdos, F. F., Yoo, S., Worthylake, D. K., Houseweart, M., Sundquist, W. I. & Hill, C. P. (1996). Crystal structure of human cyclophilin A bound to the amino-terminal domain of HIV-1 capsid. *Cell*, **87**, 1285–1294.
14. Gamble, T. R., Yoo, S., Vajdos, F. F., von Schwedler, U. K., Worthylake, D. K., Wang, H. *et al.* (1997). Structure of the carboxyl-terminal dimerization domain of the HIV-1 capsid protein. *Science*, **278**, 849–853.
15. Hill, C. P., Worthylake, D., Bancroft, D. P., Christensen, A. M. & Sundquist, W. I. (1996). Crystal structures of the trimeric human immunodeficiency virus type 1 matrix protein: implications for membrane association and assembly. *Proc. Natl Acad. Sci. USA*, **93**, 3099–3104.
16. Massiah, M. A., Starich, M. R., Paschall, C., Summers, M. F., Christensen, A. M. & Sundquist, W. I. (1994). Three-dimensional structure of the human immunodeficiency virus type 1 matrix protein. *J. Mol. Biol.* **244**, 198–223.
17. Tang, C., Ndassa, Y. & Summers, M. F. (2002). Structure of the N-terminal 283-residue fragment of the immature HIV-1 Gag polyprotein. *Nat. Struct. Biol.* **9**, 537–543.
18. Briggs, J. A., Riches, J. D., Glass, B., Bartonova, V., Zanetti, G. & Krausslich, H. G. (2009). Structure and assembly of immature HIV. *Proc. Natl Acad. Sci. USA*, **106**, 11090–11095.
19. Wright, E. R., Schooler, J. B., Ding, H. J., Kieffer, C., Fillmore, C., Sundquist, W. I. & Jensen, G. J. (2007). Electron cryotomography of immature HIV-1 virions reveals the structure of the CA and SP1 Gag shells. *EMBO J.* **26**, 2218–2226.
20. Campbell, S., Fisher, R. J., Towler, E. M., Fox, S., Issaq, H. J., Wolfe, T. *et al.* (2001). Modulation of HIV-like particle assembly *in vitro* by inositol phosphates. *Proc. Natl Acad. Sci. USA*, **98**, 10875–10879.
21. Datta, S. A. & Rein, A. (2009). Preparation of recombinant HIV-1 Gag protein and assembly of virus-like particles *in vitro*. *Methods Mol. Biol.* **485**, 197–208.
22. Gross, I., Hohenberg, H., Wilk, T., Wiegers, K., Grättinger, M. B., Müller, B. *et al.* (2000). A conformational switch controlling HIV-1 morphogenesis. *EMBO J.* **19**, 103–113.
23. Perez-Caballero, D., Hatziioannou, T., Martin-Serrano, J. & Bieniasz, P. D. (2004). Human immunodeficiency virus type 1 matrix inhibits and confers cooperativity on gag precursor–membrane interactions. *J. Virol.* **78**, 9560–9563.
24. Carlson, L. A., Briggs, J. A., Glass, B., Riches, J. D., Simon, M. N., Johnson, M. C. *et al.* (2008). Three-dimensional analysis of budding sites and released virus suggests a revised model for HIV-1 morphogenesis. *Cell Host Microbe*, **4**, 592–599.
25. Grimes, J. M., Burroughs, J. N., Gouet, P., Diprose, J. M., Malby, R., Zientara, S. *et al.* (1998). The atomic structure of the bluetongue virus core. *Nature*, **395**, 470–478.
26. Johnson, J. E. & Reddy, V. S. (1998). Biggest virus molecular structure yet! *Nat. Struct. Biol.* **5**, 849–854.
27. Goicochea, N. L., De, M., Rotello, V. M., Mukhopadhyay, S. & Dragnea, B. (2007). Core-like particles of an enveloped animal virus can self-assemble efficiently on artificial templates. *Nano Lett.* **7**, 2281–2290.
28. Loo, L., Guenther, R. H., Lommel, S. A. & Franzen, S. (2007). Encapsidation of nanoparticles by red clover necrotic mosaic virus. *J. Am. Chem. Soc.* **129**, 11111–11117.
29. Sun, J., DuFort, C., Daniel, M. C., Murali, A., Chen, C., Gopinath, K. *et al.* (2007). Core-controlled polymorphism in virus-like particles. *Proc. Natl Acad. Sci. USA*, **104**, 1354–1359.
30. Fisher, R. J., Fivash, M. J., Stephen, A. G., Hagan, N. A., Shenoy, S. R., Medaglia, M. V. *et al.* (2006). Complex interactions of HIV-1 nucleocapsid protein with oligonucleotides. *Nucleic Acids Res.* **34**, 472–484.
31. Fisher, R. J., Rein, A., Fivash, M., Urbaneja, M. A., Casas-Finet, J. R., Medaglia, M. & Henderson, L. E. (1998). Sequence-specific binding of human immunodeficiency virus type 1 nucleocapsid protein to short oligonucleotides. *J. Virol.* **72**, 1902–1909.
32. Aniagyei, S. E., Kennedy, C. J., Stein, B., Willits, D. A., Douglas, T., Young, M. J. *et al.* (2009). Synergistic effects of mutations and nanoparticle templating in the self-assembly of cowpea chlorotic mottle virus capsids. *Nano Lett.* **9**, 393–398.
33. Dixit, S. K., Goicochea, N. L., Daniel, M. C., Murali, A., Bronstein, L., De, M. *et al.* (2006). Quantum dot encapsulation in viral capsids. *Nano Lett.* **6**, 1993–1999.

34. Briggs, J. A., Simon, M. N., Gross, I., Krausslich, H. G., Fuller, S. D., Vogt, V. M. & Johnson, M. C. (2004). The stoichiometry of Gag protein in HIV-1. *Nat. Struct. Mol. Biol.* **11**, 672–675.
35. Frank, J. (2006). *Three-Dimensional Electron Microscopy of Macromolecular Assemblies: Visualization of Biological Molecules in Their Native State.* Oxford University Press, Oxford, United Kingdom.
36. Vivian, J. T. & Callis, P. R. (2001). Mechanisms of tryptophan fluorescence shifts in proteins. *Biophys. J.* **80**, 2093–2109.
37. Lacerda, S. H., Park, J. J., Meuse, C., Pristinski, D., Becker, M. L., Karim, A. & Douglas, J. F. (2010). Interaction of gold nanoparticles with common human blood proteins. *ACS Nano*, **4**, 365–379.
38. Belyi, V. A. & Muthukumar, M. (2006). Electrostatic origin of the genome packing in viruses. *Proc. Natl Acad. Sci. USA*, **103**, 17174–17178.
39. Hu, Y., Zandi, R., Anavitarte, A., Knobler, C. M. & Gelbart, W. M. (2008). Packaging of a polymer by a viral capsid: the interplay between polymer length and capsid size. *Biophys. J.* **94**, 1428–1436.
40. Bruinsma, R. F., Gelbart, W. M., Reguera, D., Rudnick, J. & Zandi, R. (2003). Viral self-assembly as a thermodynamic process. *Phys. Rev. Lett.* **90**, 248101.
41. Chang, C. B., Knobler, C. M., Gelbart, W. M. & Mason, T. G. (2008). Curvature dependence of viral protein structures on encapsidated nanoemulsion droplets. *ACS Nano*, **2**, 281–286.
42. Sorger, P. K., Stockley, P. G. & Harrison, S. C. (1986). Structure and assembly of turnip crinkle virus. II. Mechanism of reassembly *in vitro*. *J. Mol. Biol.* **191**, 639–658.
43. Nguyen, H. D., Reddy, V. S. & Brooks, C. L., III (2007). Deciphering the kinetic mechanism of spontaneous self-assembly of icosahedral capsids. *Nano Lett.* **7**, 338–344.
44. Levandovsky, A. & Zandi, R. (2009). Nonequilibrium assembly, retroviruses, and conical structures. *Phys. Rev. Lett.* **102**, 198102.
45. Bausch, A. R., Bowick, M. J., Cacciuto, A., Dinsmore, A. D., Hsu, M. F., Nelson, D. R. *et al.* (2003). Grain boundary scars and spherical crystallography. *Science*, **299**, 1716–1718.
46. Nelson, D. R. (2002). Toward a tetravalent chemistry of colloids. *Nano Lett.* **2**, 1125–1129.
47. Luedtke, W. D. & Landman, U. (1998). Structure and thermodynamics of self-assembled monolayers on gold nanocrystallites. *J. Phys. Chem.* **B102**, 6566–6572.
48. Kuna, J. J., Voitchovsky, K., Singh, C., Jiang, H., Mwenifumbo, S., Ghorai, P. K. *et al.* (2009). The effect of nanometre-scale structure on interfacial energy. *Nat. Mater.* **8**, 837–842.
49. Pornillos, O., Garrus, J. E. & Sundquist, W. I. (2002). Mechanisms of enveloped RNA virus budding. *Trends Cell Biol.* **12**, 569–579.
50. Rulli, S. J., Jr., Hibbert, C. S., Mirro, J., Pederson, T., Biswal, S. & Rein, A. (2007). Selective and nonselective packaging of cellular RNAs in retrovirus particles. *J. Virol.* **81**, 6623–6631.
51. Hurst, S. J., Lytton-Jean, A. K. & Mirkin, C. A. (2006). Maximizing DNA loading on a range of gold nanoparticle sizes. *Anal. Chem.* **78**, 8313–8318.
52. Stoeva, S. I., Lee, J. S., Thaxton, C. S. & Mirkin, C. A. (2006). Multiplexed DNA detection with biobarcoded nanoparticle probes. *Angew. Chem., Int. Ed. Engl.* **45**, 3303–3306.
53. Datta, S. A., Zhao, Z., Clark, P. K., Tarasov, S., Alexandratos, J. N., Campbell, S. J. *et al.* (2007). Interactions between HIV-1 Gag molecules in solution: an inositol phosphate-mediated switch. *J. Mol. Biol.* **365**, 799–811.
54. Campbell, S. & Rein, A. (1999). *In vitro* assembly properties of human immunodeficiency virus type 1 Gag protein lacking the p6 domain. *J. Virol.* **73**, 2270–2279.
55. Haiss, W., Thanh, N. T., Aveyard, J. & Fernig, D. G. (2007). Determination of size and concentration of gold nanoparticles from UV–Vis spectra. *Anal. Chem.* **79**, 4215–4221.
56. Ludtke, S. J., Baldwin, P. R. & Chiu, W. (1999). EMAN: semiautomated software for high-resolution single-particle reconstructions. *J. Struct. Biol.* **128**, 82–97.